Globally- vs Locally-trained Machine Learning Models for Land-slide Detection: A Case Study of a Glacial Landscape

Alexandra Jarna Ganerød *, Erin Lindsay *, Ola Fredin, Tor-Andre Myrvoll, Steinar Nordal, Jan Ketil Rød

Posted Date: 13 January 2023

doi: 10.20944/preprints202301.0231.v1

Keywords: NDVI; SAR; change detection; Norway; Sentinel-1; Sentinel-2; deep learning; U-Net; CCDC; Google Earth Engine

Article

Globally- vs Locally-Trained Machine Learning Models for Landslide Detection: A Case Study of a Glacial Landscape

Alexandra Jarna Ganerød [1,2,*,†], Erin Lindsay [3,*,†], Ola Fredin [4], Tor-Andre Myrvoll [5], Steinar Nordal [3] and Jan Ketil Rød [1]

[1] NTNU, Department of Geography; alexandra.jarna@ntnu.no
[2] NGU, Geological Survey of Norway; alexandra.jarna@ngu.no
[3] NTNU, Department of Civil and Environmental Engineering; erin.lindsay@ntnu.no; steinar.nordal@ntnu.no
[4] NTNU, Department of Geoscience and Petroleum; ola.fredin@ntnu.no
[5] NTNU, Department of Electronic Systems; torandre.myrvoll@ntnu.no
* Correspondence: alexandra.jarna@ntnu.no; Tel: +47 4512 6688
† Co-first author, these authors contributed equally to this work.

Abstract: Landslide risk mitigation is limited by data scarcity. This could be improved using continuous landslide detection systems. In order to investigate which image types and machine learning (ML) models are most useful for landslide detection in a Norwegian setting, we compared the performance of five different ML models, for the Jølster case study (30-July-2019), in Western Norway. These included three globally pre-trained models; (i) the Continuous Change Detection and Classification (CCDC) algorithm, (ii) a combined k-means clustering and Random Forest classification model, and (iii) a convolutional neural network (CNN), and two locally-trained models, including; (iv) Classification and Regression Trees and v) a U-net CNN model. Images used included Sentinel-1, Sentinel-2, digital elevation model (DEM) and slope. The globally-trained models performed poorly in shadowed areas, and were all outperformed by the locally-trained models. A maximum Matthew's correlation coefficient (MCC) score of 89% was achieved with model v, using combined Sentinel-1 and -2 images as input. This is one of the first attempts to apply deep-learning to detect landslides with both Sentinel-1 and -2 images. Using Sentinel-1 images only, the locally-trained deep-learning model significantly outperformed the conventional ML model. These findings contribute towards developing a national continuous monitoring system for landslides.

Keywords: NDVI; SAR; change detection; Norway; Sentinel-1; Sentinel-2; deep learning; U-Net; CCDC; Google Earth Engine

1. Introduction

Landslides are the most widespread geologic hazard yet are amongst the least reported type of disasters. In the period 1998–2017, landslides affected an estimated 4.8 million people globally, resulting in over 18,000 fatalities [1]. Accurate knowledge of past landslide events is needed to mitigate risk from future events, through hazard and susceptibility mapping, spatial planning and landslide early warning systems [2,3]. A lack of systematic information on the type, abundance, and distribution of historic landslides is a major limitation for landslide risk mitigation.

Landslides are generally detected from field observations, or remotely sensed imagery [4]. There have been an increasing number of studies investigating automated methods for landslide detection and mapping using machine learning (ML) models and satellite images, particularly since 2017 [5]. Operational monitoring and alert systems using similar approaches exist for deforestation [6–8], and are being developed for other types of natural hazards including flood [9] and wildfire detection

[10,11]. Similar systems for landslide detection would be extremely valuable for obtaining timely and objective data on landslide events. This would lead to improved understanding of the controlling factors and spatial distribution of past and future landslides, and improved reliability of susceptibility and hazard maps [12].

Many of the same change detection methods and data types used for continuous monitoring of forest loss are also relevant for landslide detection, given that landslides often result in removal of vegetation. Change detection with ML techniques can be performed using temporal, or spatial data from satellite images. Temporal methods can detect abrupt changes in time-series data due to a change in ground cover properties. For example, the Continuous Change Detection and Classification (CCDC) algorithm [13] can detect gradual and abrupt changes in land cover types. This works by detecting deviances from expected values, based on patterns of historic seasonal spectral behaviour for a given pixel. The original CCDC model has been run for all existing Landsat data globally, with results made available on Google Earth Engine [14]. We did not find any examples of automated landslide detection using similar time-series based change detection methods.

Spatial methods are popular for both deforestation and landslide detection. Patches of pixels showing vegetation loss can be identified from post-event, or from sets of pre- and post-event images, using various ML methods. Deep learning, and particularly, U-net architecture has proven to be a very powerful segmentation tool in scenarios with limited data, simple structure, and high recognition accuracy. These methods typically follow a workflow that involves training a model using an existing local landslide inventory. The pre-trained model is then used to predict landslides in the surrounding regions that are similar to the training area [15]. Recently U-Net has been widely used in landslide mapping, e.g. [16–20].

In terms of image types used, optical multispectral and LiDAR (light detection and ranging) data are common. However, event detection may be delayed by months due to persistent cloud cover. Hence, there has recently been an increasing use of synthetic aperture radar (SAR) data for landslide detection [21–23] and continuous monitoring systems for deforestation [6,24,25]. SAR data is also useful for change detection in areas where there are strong seasonal variations including snow, seasonal darkness, and lack of vegetative biomass (e.g., in temperate and cold climates). Using U-net architecture, a combination of both Sentinel-1 and Sentinel-2 input data, was found to achieve improved accuracy compared to optical data only, for detecting illegal logging events in both summer and winter in Ukraine. The input was stacks of optical and radar images in summer and spring, and radar images only in winter and autumn [26]. However, there are barriers to using SAR data for landslide detection, due to more complicated pre-processing, and a lack of understanding of how to interpret landslides in SAR backscatter data [23]. Therefore, most ML models for landslide detection use optical or multispectral images as input data [5].

However, even if cloud-free optical images are available shortly after a triggering event, applying U-Net models for rapid landslide mapping in emergencies is often not feasible. This is the case when there is lack of historic and local landslide data, represented as polygon features, available to pre-train the model [27]. In response to this problem, there have been attempts to produce globally-trained generalised ML models capable of detecting and mapping landslides in previously unseen locations. The first attempt was by Prakash et al., (2021) with a CNN model that was trained on seven locations around the seismically-active Pacific Ring, with high vegetation coverage. Another example was Tehrani et al. (2021) who developed an object-based method using k-means clustering to perform semantic segmentation, followed by Random Forest classifiers, that determine whether the segments represent landslides or not. This model was trained on data from 29 locations around the world.

In this study, our main goal is to determine which elements of existing automatic landslide detection and deforestation monitoring approaches could be feasible to include for a national landslide detection system in Norway. This represents one of the first attempts to use ML to detect and map landslides in Norway. With a glacially-formed landscape, and strong seasonal variability, the environment in Norway is relatively unique, and it is unknown how well the generalised models will perform in such a setting. We investigate the performance of five different ML models using satellite images from Sentinel-1 and -2, along with elevation and slope rasters. The well-verified

 doi:10.20944/preprints202301.0231.v1

landslide inventory from the Jølster case study (30-July-2019) is used, to test which approaches could be adapted for larger scale use in the future.

We test the performance of three pre-existing globally-trained models, including (i) the time-series based CCDC algorithm, (ii) the object-based model from Tehrani et al., (2021) and (iii) the pixel-based CNN model from Prakash et al., (2021). Two locally trained models were also tested including; (iv) a Classification and Regression Tree (CART) ML model [28], and (v) a CNN U-net DL model.

The following research questions are investigated:

1. How do globally pre-trained ML models for landslide detection perform in a glacial landscape?
2. Which locally-trained model and input data combination gives the best results?
3. Which elements of the investigated models could be implemented in an operational national landslide detection system?

In the following section, we describe the current situation for Norway in terms of landslide hazards and introduce the case study. In the results section we show that the globally-trained models generally did not perform well in a glacial landscape, particularly for landslides on north-facing slopes. The locally-trained DL-model outperformed the ML model with all input data combinations, except for one. The best performance (MCC score: 89%) was achieved using combined Sentinel-1 and Sentinel-2 data as input. We did not attempt to retrain or modify the existing pre-trained globally-trained models in this study, although we provide suggestions as to how the performance could be improved in the discussions.

2. Norway Setting and Case Study

Landslides occur almost daily in mountainous regions in Norway and are the natural hazard responsible for most fatalities [29]. In addition, they cause large economic losses due to damages to infrastructure, and disruption to transportation [30]. In comparison to other countries in Europe, Norway has a relatively high proportion of land area that is susceptible to landslides, with over 70% of municipalities affected [31]. This is due to the geological landscape with high mountains, valleys with steep slopes, and post-glacial isostatic rebound that has resulted in sensitive clays in valley bottoms in coastal regions [29].

The most frequent type of landslides in Norway include rock fall, rock slides, debris avalanches, and debris flows [12]. In addition, there are unstable mountains and deep-seated landslides, that can evolve into large rock avalanches, and quick clay slides [29].

In order to mitigate the increasing risk to society due to landslide hazards, there are several national initiatives coordinated by the Norwegian Water Resources and Energy Directorate (NVE). These include, among others, the preparation of susceptibility and hazard maps and a close communication with spatial planners at municipalities, in order to protect inhabitants and key infrastructure already located in hazardous areas. NVE is also working with prediction of hydro-meteorologically induced landslides occurrences, through a national early forecasting and warning service [7,8]. The early warning system allow municipalities and individuals to take timely action to reduce risk, including evacuations, and closure of transport routes in areas with high hazard.

These initiatives rely on knowledge of historic landslide occurrence, and are limited by the quality and completeness of historic landslide records [12]. The Norwegian Mass Movements Database (available from: https://nedlasting.nve.no/gis/, accessed 20-Dec-2022) contained 84,768 reports at the time of writing, from the year 900 to 2022. Yet there are some significant limitations in the existing landslide dataset that make it unsuitable for spatial analyses, for instance determining statistical relationships between landslide occurrence and the topographical, geological, hydrological, vegetation or meteorological factors. These include low spatial location and qualitative (i.e., information on landslide type, size, trigger) accuracy of older events that have been extracted from historic church and municipality records. These reports are generally limited to events that caused death or destroyed property.

While modern reporting is performed systematically by the road and rail authorities [32], reporting focuses on events that directly impact transport infrastructure. The given locations are typically represented with the point where a landslide impacted the road, and the initiation point is

Preprints (www.preprints.org) | NOT PEER-REVIEWED | Posted: 13 January 2023 doi:10.20944/preprints202301.0231.v1

not usually specified. Although this data generally has high spatial and temporal accuracy, there remains some qualitative inaccuracies. Furthermore, compared to 11 other national landslide databases, there is a spatial biased distribution with many reports located along roads but relatively few events reported in remote areas [33], as illustrated in Figure 1.

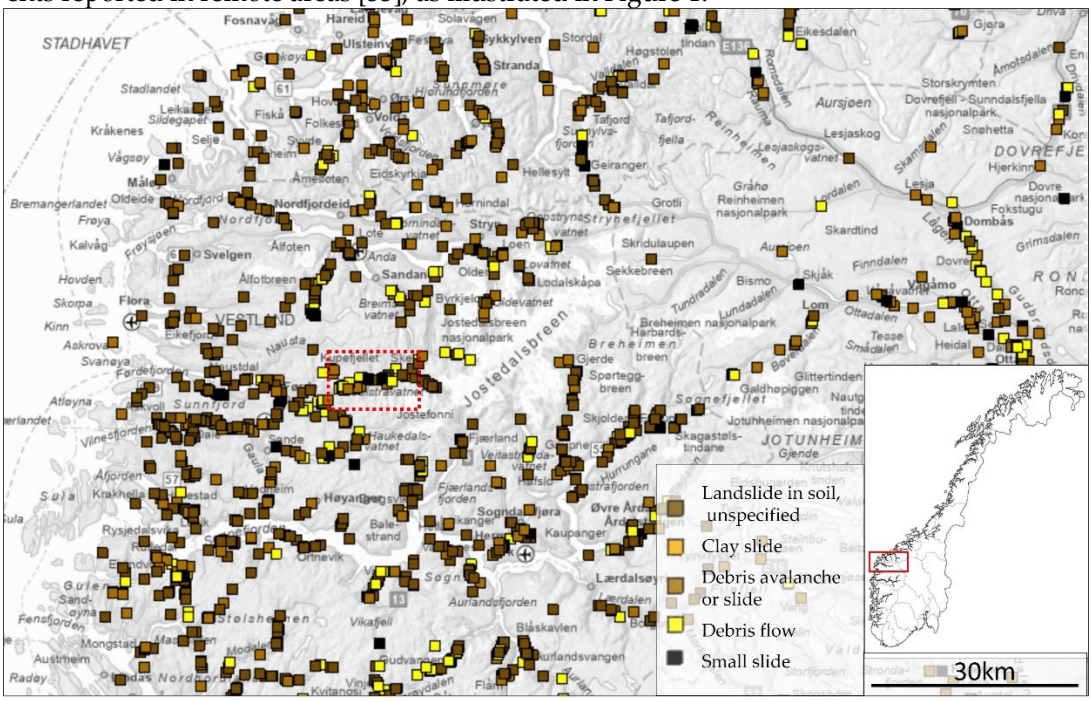

Figure 1. Registered landslide events in Western Norway have an inherent spatial bias towards roads. The study area of Jølster is shown by the dashed red lines. Data from www.skredregistering.no (accessed: 16-Dec-2022), showing registered landslide events from 1992 to 2022.

There is a strong need for improved landslide mapping techniques in Norway, which can provide objective and accurate spatial information, and also allowing the detection of events that occur away from populated areas and transport routes. Recent studies have demonstrated there is great potential to improve detection of landslides in remote areas using satellite images [34,35].

In July 2019, an extremely heavy rainfall event triggered multiple landslides in the (formerly named) Jølster municipality in Western Norway [34]. The road authority reported 14 landslides on this date, while mapping from Sentinel-2 images detected 120 events, with only 30% being located within 500 m of a road, compared to 100% of those registered by the road authority [35]. NVE used aerial and satellite images to manually map polygons representing the landslide and performed a quality control of the existing landslide point data. However, detecting and mapping traces of small landslide events across large areas, remains a tedious and labour-intensive process [36].

The study area is shown in Figure 2. The landscape consists of steep glacial valleys, lakes and mountains up to 1666m. Jølster is located in a temperate climate zone. The bedrock geology is predominantly granitic (banded and augen) orthogneiss and quartz-monzonite. The geomorphology is shaped by old faults and glacial erosion, with a quaternary surface cover typically consisting of highly consolidated moraine material overlying the bedrock, with a looser veneer of colluvium on valley slopes. The surface cover is thin to non-existent at high altitude and increases to several meters thick in lower areas close to the lake. The vegetation ranges from sparse moss and shrubs or light birch forest at high elevations, to spruce forest and agricultural fields lower in the valleys. Roads and built areas are mainly located in the flatter main valleys. The area is very susceptible to landslides due to the steep slopes and wet climate, with over 40 historic landslides recorded in the national database [35]. The hydro-meteorologically induced landslides that pose risk to these areas are expected to become more frequent due to an increase in extreme precipitation events [37].

Preprints (www.preprints.org) | NOT PEER-REVIEWED | Posted: 13 January 2023 doi:10.20944/preprints202301.0231.v1

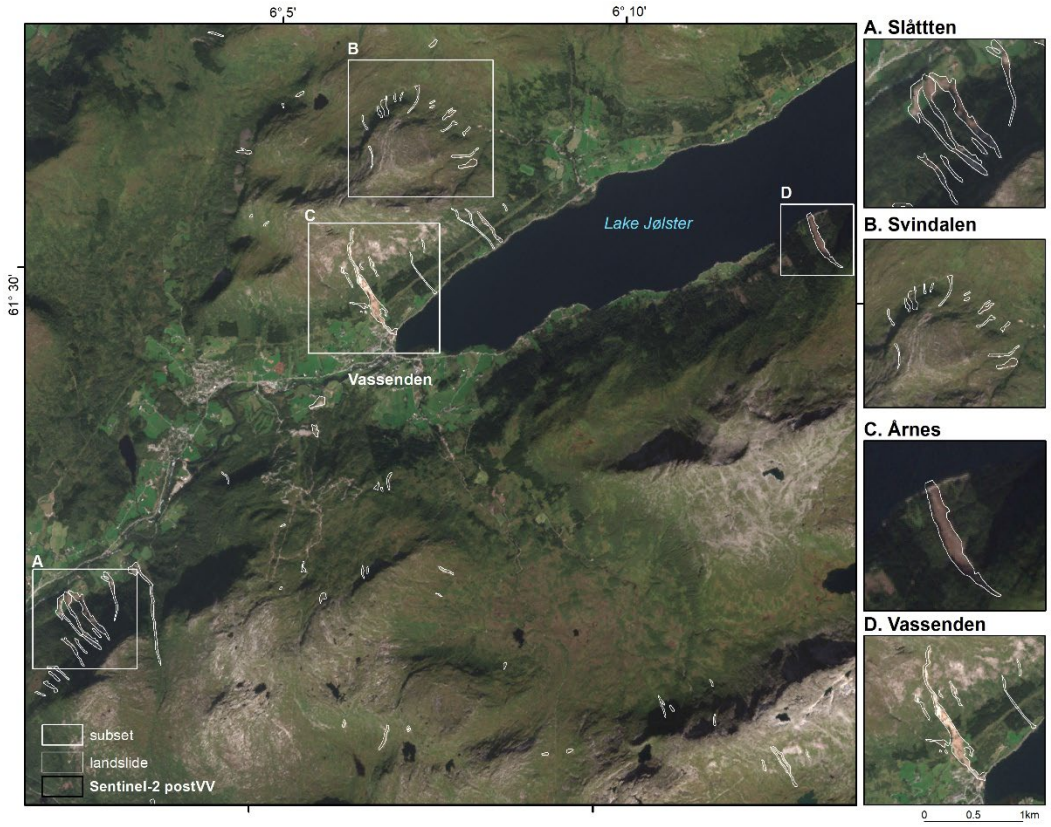

Figure 2. Case study overview showing four subsets with ground truth landslide outlines in white.

3. Methods

We compare the performance of three different models: (a) generalized global predictive models (Tehrani, Prakash), (b) supervised machine learning models in Google Earth Engine (GEE) (smile.Cart classifier), (c) pixel-based deep learning model (U-net). For verification of the results, we used a set of 120 manually mapped landslides from [35].

3.1. Generalized Globally Trained Predictive Models

In order to run the three generalized predictive models, the steps in the methods and accompanying documentation on GitHub were followed, with some modifications made where necessary. A brief summary of these methods and any deviations are described here.

CCDC model (available: https://github.com/parevalo/gee-ccdc-tools): The CCDC model results are available for visualization purposes as an app on GEE, however the global dataset is not yet publicly available yet. The results from the global CCDC dataset were provided on request for use in this study [48]. The results have been pre-calculated for the Landsat bands (not including NDVI). The SWIR1 band was chosen for the change detection analysis, as this is known to be sensitive to changes in vegetation. The changes within the period 1-Jul-2019 to 31-Aug-2019 were displayed for the study area using the app.

Tehrani model (available https://github.com/giosans/multiregional-landslide-detection-article): pre-processing of the input data is done automatically using a script run in GEE, described in detail in the master thesis '*Landslide Detection using Random Forest Classifier*' [38]. The script takes a table of landslide coordinates and dates, and generates sets of Geotiff images for each point, that are then used as input for the ML model. Sentinel-2 Level 1C images with low cloud coverage are selected, within three months before and after the landslide event date. If no cloud free images are found in that period, a composite image is made using images from one year. The pre-processing involves normalization of the images, and addition of brightness, NDVI and GNDVI (green-NDVI) bands, and the output is three images for each landslide point; pre-event, post-event and difference (see Figure

Preprints (www.preprints.org) | NOT PEER-REVIEWED | Posted: 13 January 2023 doi:10.20944/preprints202301.0231.v1

3I). Modifications made to this process included uploading a shapefile to GEE, instead of a Google Fusion table, which has been discontinued. Also, the 10 m resolution Norwegian DTM was used instead of the global 30 m resolution ALOS DEM, because the ALOS DEM does not cover Norway.

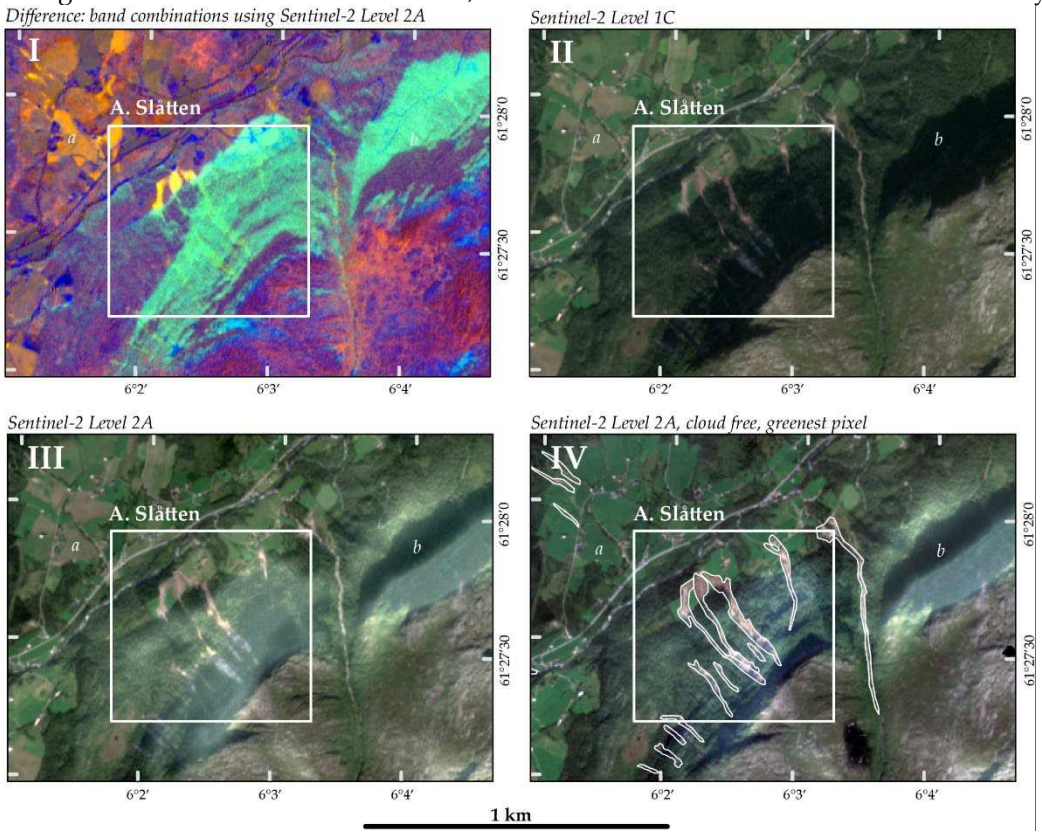

Figure 3. Optical image inputs derived from Sentinel-2 images shown for subset A. at Slåtten. **I**. Difference image with three bands (brightness, red-over-green and NDVI derived from Level-2A images) used for the Tehrani model. **II.** Sentinel-2 Level 1A Top of Atmosphere (TOA). **III**. Sentinel-Level 2A, with atmospheric correction applied to the Level-1C TOA image. Note that the shadowed areas at point b have been brightened. **IV**. Cloud-filtered, greenest-pixel composite produced from Sentinel-2 Level2A images. Images II-IV were used as inputs in the Prakash-model, while the locally-trained model based on U-net architecture used only image IV, along with Sentinel-1 images.

The images were then added to the landslide detection model available as a python code, which was run using Microsoft Visual Studio Code (VSC). The outputs are raster images with labelled segments in KEA file format, and a list of the segments that were classified as landslides.

Prakash model (*available https://github.com/nprksh/landslide-mapping-with-cnn*): The required inputs are three band (R, G, B) pre- and post-event images, and single-band slope, hillshade, DEM, bounding box and no-data mask rasters. In the accompanying paper, it was not specified if Sentinel-2 Level 1C, or Level-2A products were used. Pre-processing the input images involved selecting a Sentinel-2 image at the landslide location with the lowest cloud cover within one month of the landslide date, clipping to the area of interest, and then manually creating a mask of snow and clouds. Again, we used the Norwegian DTM instead of a global DEM, from which slope and hillshade images were created. The model was also available as a python script, that links to a remotely stored Tensor Flow model. This was again run in VSC, and the outputs were geotiffs of predicted landslide pixels.

Greenest-pixel composite image: One modification to the methodology described in Prakash et. al, 2021, was to use a greenest-pixel composite as input, as this method can reduce noise from clouds and agriculture. These were produced using one month of images from before and after the landslides, using the S2 cloudless algorithm for cloud filtering, and the SCL (scene classification) band for snow filtering. Using the quality mosaic function, a composite image was then created based on NDVI, in which for each pixel – the pixel with the maximum NDVI is taken, along with the

Preprints (www.preprints.org) | NOT PEER-REVIEWED | Posted: 13 January 2023 doi:10.20944/preprints202301.0231.v1

corresponding values from the other bands from the same date. This gives a 'greenest pixel' composite that is cloud-free and gives the least snow cover and shadow within the specified date range.

3.2. Locally-Trained Supervised Machine Learning Model in GEE

Landslide predictions were performed in Google Earth Engine using the ee.Classifier.smileCart algorithm [28], which uses a CART (Classification and Regression Trees) classifier. This involved the following steps.

First, the images were pre-processed. For Sentinel-2, one month of Level-2A images from before and after the event were used to create cloud-filtered, greenest-pixel composites. The cloud filtering was performed using the s2cloudless algorithm to remove cloudy pixels (see: https://developers.google.com/earth-engine/tutorials/community/sentinel-2-s2cloudless, accessed: 08-Dec-2022). Greenest-pixel composites were then created from the pre- and post-event image collections, using the qualityMosaic() function. For each pixel in the image, the qualityMosaic() function selects the image with the highest NDVI value to contribute to the resulting composite image. All bands from the same image the selected pixel with the highest NDVI value was taken from, are included in the output. For Sentinel-1, again one month of images, from pre- and post-event were used to create terrain-corrected median composites. The terrain correction was performed using the approach from ref [39] using the volumetric scattering model. Then median-composites for VV and VH bands separately, were created from each of the pre- and post-event image collections, using both ascending and descending orbit geometries. Finally, the Sentinel-1 and –2 bands were combined along with elevation and slope, into a single 13-band image.

Secondly, the supervised classification was performed, following the tutorial by S. Levick (https://www.gears-lab.com/intro_rs_lab4/, accessed: 08-Dec-2022). This involved selecting training points from which to train the classifier. 18 points were manually selected in the landslide class, and 112 points from seven different non-landslide classes (water, snow/ice, bare soil/rock, agriculture, forest, alpine scrub, and urban). Care was taken to sample from diverse slope aspects, elevations, and within shadow areas. The 13-band image was then sampled at each point, and these values were used to train the classifier and perform a classification across the whole image. In addition, classifications were performed using the same points, for a 3-band, and 2-band subsets of the full 13-band image, as shown in Table 1.

Table 1. Input data used in locally-trained models for four different settings.

Model run	No. of bands	Bands
S1, S2 & DEM	13	Sentinel-1: pre-VV, post-VV, diff-VV, pre-VH, post-VH, diff-VH
		Sentinel-2: post-R, post-G, post-B, post-NIR, dNDVI
		Terrain: elevation, slope
S1 (VV) & S2	3	Sentinel-1: pre-VV, post-VV
		Sentinel-2: dNDVI
S1 (VV) only	2	pre-VV, post-VV
S2 only	5	post-R, post-G, post-B, post-NIR, dNDVI

The results were inspected to see if any misclassification was apparent. Then finally, a binary image of landslide-non-landslide was produced by combing the non-landslide classes, and salt-and-pepper noise reduced using the focalmode() function.

3.3. Localy Trained Pixel-Based Deep Learning Model

The entire algorithm was then implemented in a Jupyter Notebook using ArcPy, Keras and TensorFlow 2. The chosen model is a scaled- down version of deep-learning architecture called U-net, deep-learning architecture for automatic semantic segmentation [40] with Keras implementation.

Preprints (www.preprints.org) | NOT PEER-REVIEWED | Posted: 13 January 2023 doi:10.20944/preprints202301.0231.v1

Keras is an open-source software that provides python inference for artificial neural networks needed for TensorFlow 2 library [41]. The U-net is a convolutional network architecture for fast, effective, and precise segmentation of images with its symmetric U-shape. U-net has proven to be a powerful segmentation tool in scenarios with limited data, simple structure, and high recognition accuracy. The network is based on the fully convolutional neural network (FCNN) for semantic segmentation [42]. A CNN can learn deep (hierarchical) feature representations of an image, by what it enables to perform classification tasks directly from images [43].

For the training data sequence, we used random sampling of classified tiles. During the training process, an input image flows through the CNN network that recognize it with a set of trainable kernels, resulting in a group of feature maps [44]. For each of the three settings we generated minimally 10,000 sample chips using Image Analyst license and ArcGIS Pro (ArcGIS Pro, 2022). The best suitable tile size in our case was 128x128 and stride (the distance to move in the x,y direction when creating the next image chips) of 64x64 to have 50% overlap in each sample chip. The output was a dataset of classified image tiles, the format primarily used for pixel classification. The dataset was then divided into training, validation and test subsets. The trained model was saved as a 'Deep Learning Package' ('.dlpk' format), which is the standard format used to deploy deep learning models on the ArcGIS platform. The same input dataset was used as for the GEE smile.CART model described in Section 3.2.

3.3. Performance Evaluation:

The landslide inventory produced from the S2-BT image was used for verifying the results of the other approaches.

Qualitative and quantitative analyses: The results of the CCDC and Tehrani models are briefly described in a qualitative manner, as both these methods produced limited landslide predictions. Additionally, it was not possible to download the CCDC model results from the GEE app, therefore it was not possible to do quantitative pixel scale analyses on these results.

The Prakash model run results were evaluated quantitatively, as follows. The landslide polygons mapped with Sentinel-2 dNDVI were converted to a binary raster. This was used to compare with the automated landslide detection model outputs. Following the remaining approaches, a map of confusion matrix values was created, showing true positive (TP), false positive (FP), false negative (FN) and true negative (TN) values. From these, the performance metrics precision, recall, F1-score and MCC scores were calculated (see Table 2). Since landslides represent only a tiny fraction of all the pixels in the study area, the learning problem is highly imbalanced towards non-landslide pixels. Therefore, the accuracy score can become unreliable due to the large proportion of true negatives. The MCC score is considered to be the most appropriate metric for comparing the results [45]. For a binary model, the MCC gives a score between 0 to 1; with 0 indicating a model with no correlation (random predictions) and 1 indicating a perfect correlation (all correct predictions).

Table 2. Equations for performance evaluation metrics from confusion matrix values.

Metric	Formula
Precision	$\frac{TP}{TP + FP}$
Recall	$\frac{TP}{TP + FN}$
F1-score	$\frac{2TP}{2TP + FP + FN}$
MCC	$\frac{TP \times TN - FP \times FN}{(TP + FP)(TP + FN)(TN + FP)(TN + FN)}$

4. Results

The performance of the three globally-trained, and two locally-trained, ML models in the Jølster case study is presented in this section.

Preprints (www.preprints.org) | NOT PEER-REVIEWED | Posted: 13 January 2023 doi:10.20944/preprints202301.0231.v1

4.1. Globally-Trained Models

4.1.1. CCDC model-(i):

The CCDC model detected the large Vassenden landslide quite precisely (Figure 4), along with one other debris flow to the east. The large landslides at Årnes and Slåtten were not detected, nor were any of other the smaller landslides in the study area.

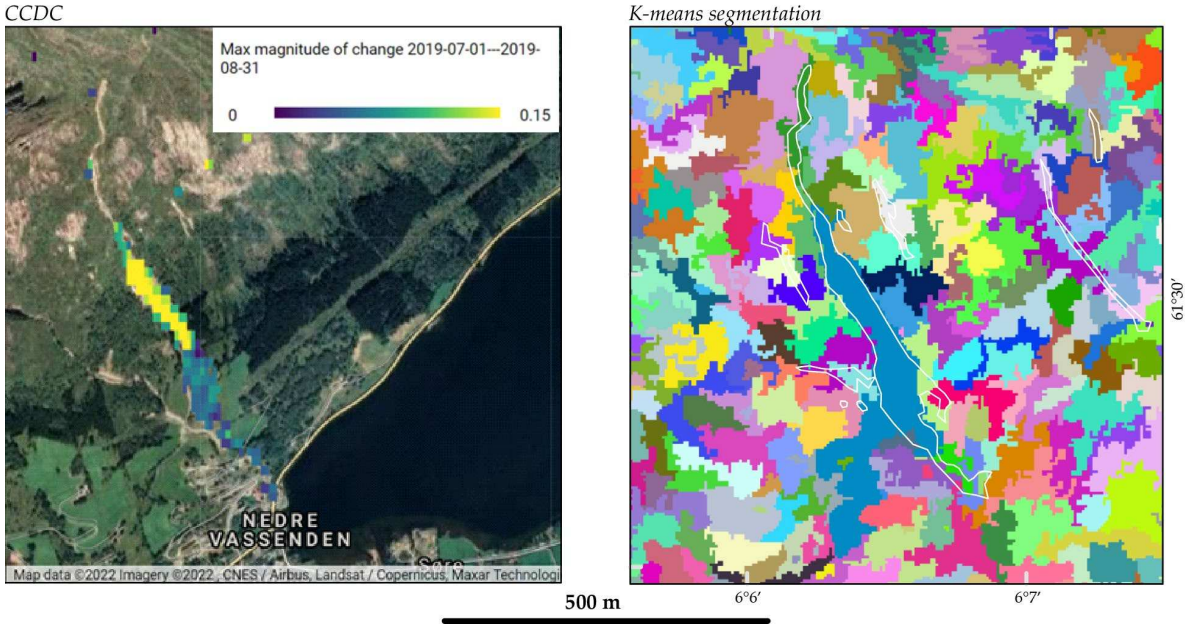

Figure 4. Results of CCDC and Tehrani models. Left: CCDC results: NDVI band change detection between July 1st and August 31st 2019. CCDC results included with permission (Arévalo, P.; pers. comm. 2022). Right: Output results of k-means segmentation. White polygon outlines show the manually mapped landslides used for verification.

4.1.2. Tehrani Model-(ii):

Overall, no landslides were detected using this model. The large landslide at Vassenden was partially segmented (see Figure 4), although the initiation zone was missed, and some nearby fields were included. The deposits of the landslides at Slåtten were also segmented. However, no segments were classified as a landslide.

4.1.3. Prakash Model-(ii):

The Prakash model was run with three different variations of Sentinel-2 images shown in Figure 3 (1) Level 1C, (2) Level 2A, and (3) a cloud-free greenest-pixel composite. The results are shown as confusion matrix maps in Figure 5. The most striking differences between the runs were firstly, that many false positives (wrongly predicted as a landslide) appear in the Level 2A products, and secondly, in the Level 1C product, there are many false negatives (missed landslides).

Preprints (www.preprints.org) | NOT PEER-REVIEWED | Posted: 13 January 2023 doi:10.20944/preprints202301.0231.v1

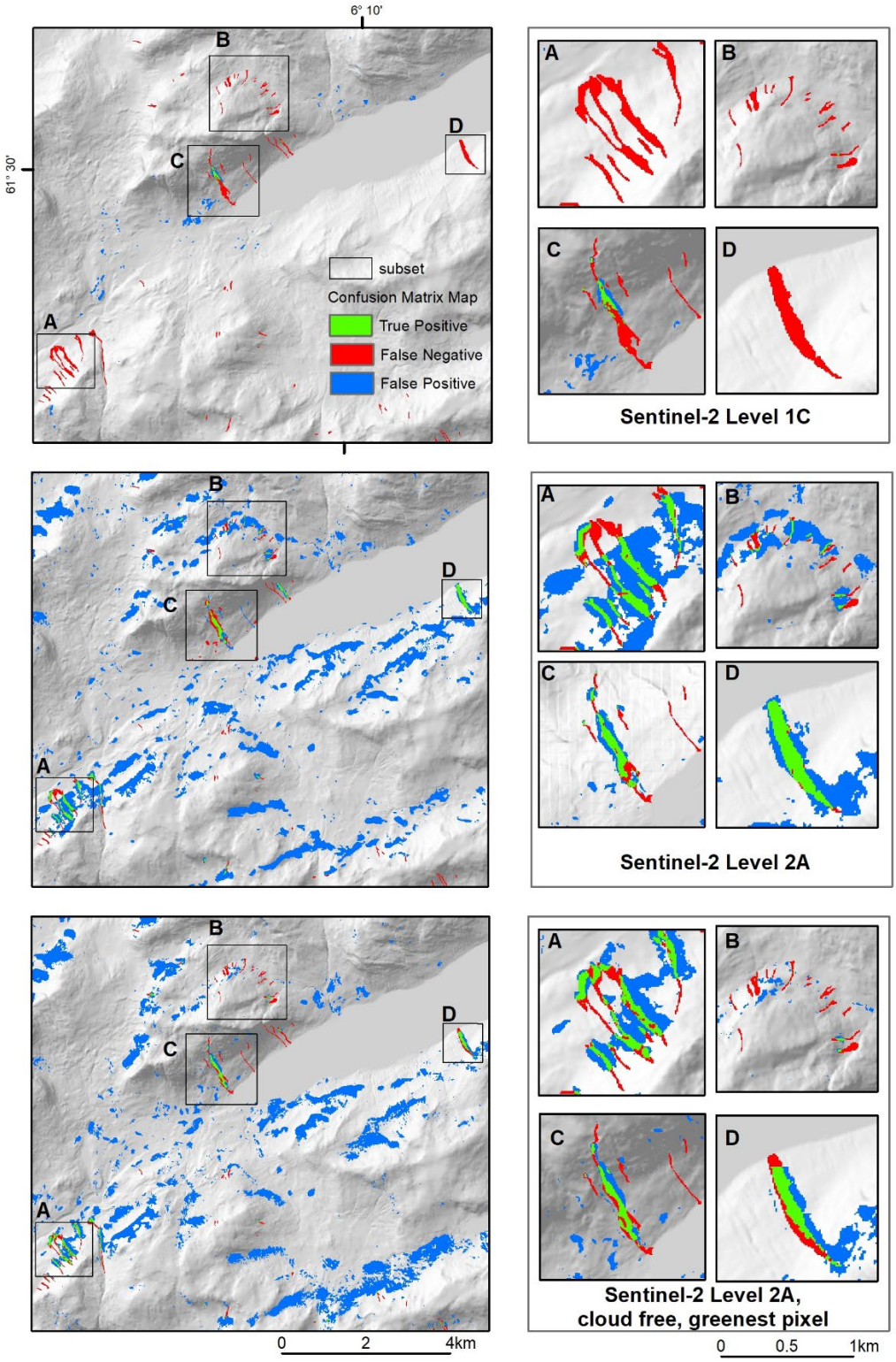

Figure 5. This figure shows three different layer settings: (1) Level 1C, (2) Level 2A, and (3) a cloud-free greenest-pixel composite.

After closely inspecting the results, it was noticed that the false positives in the Level 2A results appeared to be related to unnaturally bright areas on the northern slopes. This turned out to be due to an anomaly resulting from the terrain correction used in processing the Level 2C products, that results in blueish appearance in shadowed areas in true colour composite images, and inaccurate surface reflectance values [46]. The problem has been reported to the Sentinel-2 Quality Working Group (December 2021) [47]. An outcome of their analysis is expected in the near future, changes will be

Preprints (www.preprints.org) | NOT PEER-REVIEWED | Posted: 13 January 2023 doi:10.20944/preprints202301.0231.v1

reported in the Sentinel 2A Data Quality Report, (available from: https://sentinel.esa.int/web/sentinel/user-guides/sentinel-2-msi/document-library). Due to the noise introduced by these artefacts, comparing the performance metrics of the model runs over the entire study area was not very insightful. Therefore, for more detailed comparison, the metrics were calculated for the sub-plots shown in Figure 5. These are shown in Table 3.

Table 3. Prakash model-(iii) performance metrics. The metrics were calculated for the entire study area, as well as for the four subplots shown in Figure 7. The model was run with three different inputs; 1. Level-1C images, 2. Level-2A images, and 3. Level-2A images as a cloud-free, greenest pixel composite. The MCC score (Matthew's Correlation Coefficient) is considered the most representative metric for the imbalanced problem of landslide classification [45].

Location	Model run	Precision %	Recall %	F1-score %	MCC %
Entire area	1 - S2_L1C	5	4	4	4
	2 - S2_L2A	2	45	5	9
	3 - S2_L2A_gr	2	37	4	7
A. Slåtten	1 - S2_L1C	40	0	0	2
	2 - S2_L2A	19	60	29	20
	3 - S2_L2A_gr	30	58	40	33
B. Svidalen	1 - S2_L1C	86	1	1	8
	2 - S2_L2A	6	28	9	8
	3 - S2_L2A_gr	8	6	7	5
C. Vassenden	1 - S2_L1C	25	17	21	18
	2 - S2_L2A	40	51	45	43
	3 - S2_L2A_gr	35	46	40	37
D. Årnes	1 - S2_L1C	-	0	0	-
	2 - S2_L2A	33	96	49	51
	3 - S2_L2A_gr	35	60	44	41

For the entire study area, the MCC scores are below 0.1. In the subplots, there are false positives likely caused by the over-correction artefact in the results for B, C, and D, which are on north facing slopes. Despite this, the best score was 0.51 for model run 2, in the subplot D (Årnes landslide). The second best was 0.43 for model run 2, in the subplot A (Vassenden landslides). Subplots B (Svidalen) and C (Slåtten) had poor results across all runs.

In the first run, with Level-1C images, overall, the model failed to detect landslides. Only a small part of the Vassenden landslide was detected. The large landslides on north-facing slopes were not detected at all. There were some false positives, mainly related to changes in agricultural areas.

In the second and third runs, with Level 2A images, the model predicted the Vassenden and Årnes landslides fairly well. In subplot C (Vassenden), there are more false positives in run 3 in agricultural areas than in run 2. These results are more likely to be meaningful because the slope is south-facing and not affected by the over-correction artefacts. In subplot B (Årnes), there are slight differences in the number of false positives between the two runs, however it is difficult to say whether the difference is related to the artefacts or to the difference between the manually masked image (run 2), and the greenest-pixel composite (run 3). The landslides in subplot A (Slåtten) were partially detected with the Level-2A images. However, most of the predictions on the steep north-facing slopes are false positives due to noise, while the deposit of the western-most of the three debris flows seems to have been detected correctly. It is interesting that that particular deposit was detected, and not the other two, given that from field observations the deposits of the western-most debris flow were noticeably different from the others. The western-most deposit was a very thin layer of soil, with a high concentration of washed-out light-coloured boulders and stones, whereas the other two were much thicker (up to 2 m high) deposits consisting of darker soil and forest debris (seen here). Finally, in subplot D (Svidalen), there is a significant difference in the number of false positives, with much fewer in the greenest-pixel composite from run 3, compared to run 2. Again, it is not clear if this difference is due to the artefacts or pre-processing. There appears to be just one pixel that has

Preprints (www.preprints.org) | NOT PEER-REVIEWED | Posted: 13 January 2023 doi:10.20944/preprints202301.0231.v1

been correctly identified in all three runs. However, overall, the model was not able to detect the smaller landslides.

Despite the mediocre performance in these model runs due to introduced image artefacts, this model shows potential. With different adjustments, such as using input images without the over-corrected shadow areas, and including NDVI or Sentinel-1 bands, to make the classification more robust in shadowed areas, the model performance could be improved.

4.2. Locally-Trained Models

4.2.1. CART Model-(iv)

For the second approach, supervised machine learning model in GEE with the application of ee.smile.Cart classifier, was tested with different layer settings. We can conclude that despite a more time-consuming data preparation with defining all the different classes were some of the layer's combination giving very promising predictions. Mostly second combination of layers (dNDVI, pre-event images, post-event images).

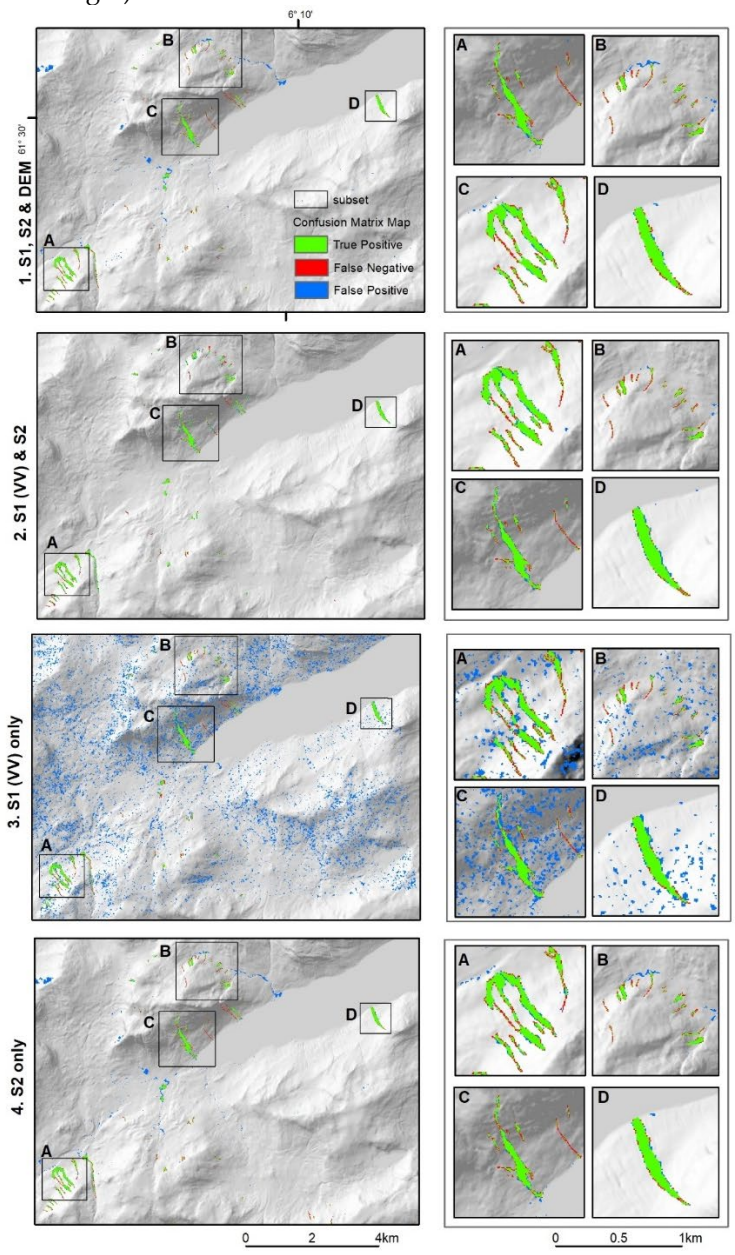

Figure 6. This figure shows three different layer settings: (1) full version (all 13 bands) (2) dNDVI, preVV, postVV (3) preVV, postVV (4) post-R, post-G, post-B, post-NIR, dNDVI.

Preprints (www.preprints.org) | NOT PEER-REVIEWED | Posted: 13 January 2023 doi:10.20944/preprints202301.0231.v1

Table 2. Performance metrics for landslide detection for locally-trained models, using four different input data combinations.

MODEL		Setting 1	Setting 2	Setting 3	Setting 4
		S1, S2 & DEM	S1 (VV) & S2	S1 (VV) only	S2 only
iv) CART	precision %	62	72	6	59
	recall %	73	74	72	72
	F1 %	67	73	11	65
	MCC	63	73	20	65
v) U-Net CNN	precision %	80	83	85	84
	recall %	33	79	74	73
	F1 %	47	81	79	78
	MCC	51	89	79	78

4.2.2. U-Net CNN Model-(v)

The third approach, locally trained deep learning model with the use of keras, tensor flow 2 and U-net architecture, is showing very promising predictions. The prediction values for all three settings showing precision results between 80-85%. The setting 2, combinations including both Sentinel-1 (pre- and post-event images) and Sentinel-2 (dNDVI) datasets are showing the highest values for recall (79%) and MCC (89%) and best visual prediction (Figure 7). The values for MCC vary from 51-89%. The highest values for F1 score are pointing towards the second setting with 81% and for Setting 3 79%. The resulting prediction for all three settings from all three approaches can be seen at the Figure 7. The Matthew's coefficient. The predictions introduce significant amounts of mostly false negatives (red) with poor prediction results based on Setting 1 with all 13 bands. All the small sized landslides are in this setting not predicted. On the other hand, with the use only Sentinel-1 pre- and post-even images in Setting 3, in A.Slåtten, is visibly not predicted upper part of the landslides. Most of the landslides are predicted correctly however with some missing pixels around which were not predicted as a landslide (FN). In summary, the prediction values and visibly with most of the pixels predicted as a landslide is based on Setting 2.

Preprints (www.preprints.org) | NOT PEER-REVIEWED | Posted: 13 January 2023 doi:10.20944/preprints202301.0231.v1

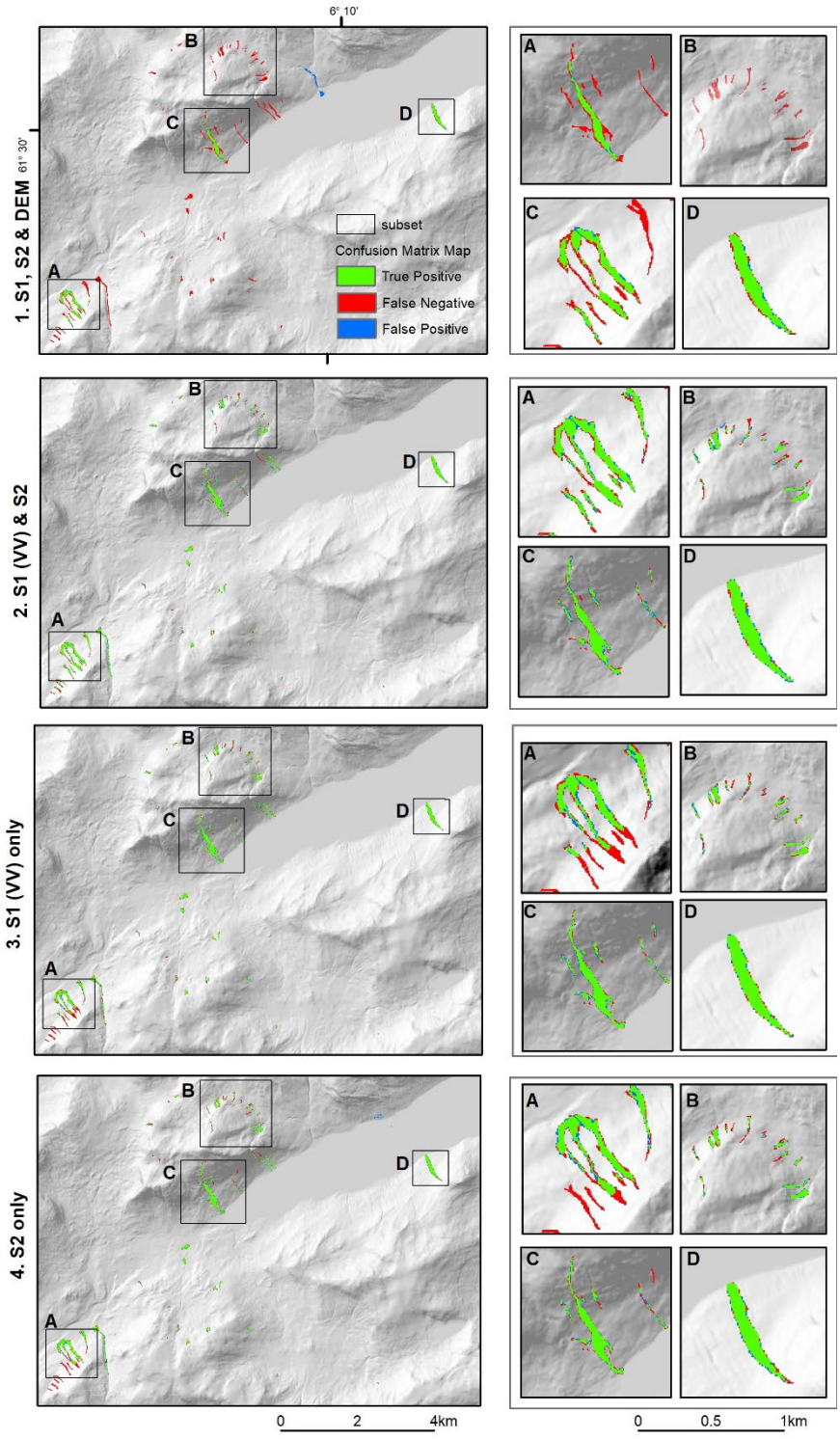

Figure 7. This figure shows three different layer settings: (1) full version (all 13 bands) (2) dNDVI, preVV, postVV (3) preVV, postVV (4) post-R, post-G, post-B, post-NIR, dNDVI.

5. Discussion

5.1. Performance of Globally Pre-Trained ML Models in a Glacial Landscape

Overall, the generalized models tested did not perform very well. Only the largest landslides were detected by these models. In most of the tests, the results appeared to be affected by slope aspect, and over-correction of shadow artefacts on north-facing slopes in the Sentinel-2 Level-2A products.

Preprints (www.preprints.org) | NOT PEER-REVIEWED | Posted: 13 January 2023 doi:10.20944/preprints202301.0231.v1

The CCDC model-(i), despite not being designed specifically for landslide detection, showed good potential for applying time-series based change detection methods for continuous landslide monitoring. The large landslide at Vassenden was outlined quite precisely, within the 30 m resolution of the Landsat data. However, it failed to detect the large landslides on north-facing slopes (i.e., in subsets A. Slåtten, and C. Årnes), and only detected one other landslide clearly. The results were very simple to view using the Google Earth Engine app [4]. Furthermore, by extending the time-period visualized, the app allowed the user to quickly identify other landslides outside of the study area, which occurred within the past 20 years. Although CCDC is designed for monitoring land cover changes generally [13], some modifications (e.g., running with NDVI, and Sentinel-2, and perhaps Sentinel-1 data) could enable it to be used as part of a continuous landslide monitoring service.

Using the Tehrani model-(ii), only the large landslide at Vassenden was visible in the segmentation results, although it was not classified as a landslide. This method used the Sentinel-2 Level-1C images as input. From the different runs with the Prakash model it was observed that the landslides are detected more frequently when using the atmospherically corrected Level-2A products compared to Level-1C, especially for landslides on north facing slopes. Thus, it can be speculated that the landslide detection on north-facing slopes may have been improved by using the Level-2C product. However, as seen from the results of the Prakash model runs with Level-2C product, the anomalies caused by terrain over-correction on shadowed areas, using the Level-2C product may also have introduced false positive predictions. The Tehrani model was also trained using landslides that were over 1000 km^2, and the minimum size of pixel clusters was 80. Including more small landslides in the training data set, and adjusting the minimum size of pixel clusters, may improve the detection of smaller landslides. Adjusting the number of k-means, or perhaps training with different indices, may improve the performance of the random forest classification.

The performance of the Prakash model-(iii) was strongly affected by the Sentinel-2 product type, with very limited correct landslide detection with Level-1C (high levels of false negatives), and improved landslide detection with Level-2A, however with the introduction of significant areas of false positives due to the terrain over-correction anomaly. Due to these false positives, the difference between using the single image inputs (run 2), compared to the greenest-pixel cloud composite inputs (run 3) was not clear, even when examining the image at the resolution of the subsets. The landslide predictions were not as precise as in the CCDC and Tehrani models. To better understand the performance of this model using different inputs, it is recommended to wait for the reprocessing of the Sentinel-2 Level 2 images. This model could potentially be improved by retraining the classifier with more Norwegian landslide data, and by including a greater range of bands and vegetation indices.

5.2. Comparison of Locally-Trained ML and DL Models and Input Data Combinations

The U-net DL model-(v) outperformed the CART ML model-(iv) for three out of four input data combinations. These findings are in agreement with similar ML vs DL model comparison studies for landslide detection [48,49]. The best MCC score achieved for our study area was 89%, using the three-band combination of pre-VV and post-VV from Sentinel-1, and dNDVI from Sentinel-2. In both the S1-only and S2-only input data settings, we that the model could not recognise the landslide signature in the initiation zones of the landslides at Slåtten (subset A). We did not find any other landslide detection studies in the literature, where both Sentinel-1 and -2 data have been used to train a DL model. However, our results are in agreement with a similar study on illegal logging detection [26].

For S2-only DL, the false negatives appear in the shadowed area. The signature of the landslides is very clear from the dNDVI image only, even where shadows are present (Figure 8). It is possible that the inclusion of RGB bands reduces the performance of the classifier in this area.

Preprints (www.preprints.org) | NOT PEER-REVIEWED | Posted: 13 January 2023 doi:10.20944/preprints202301.0231.v1

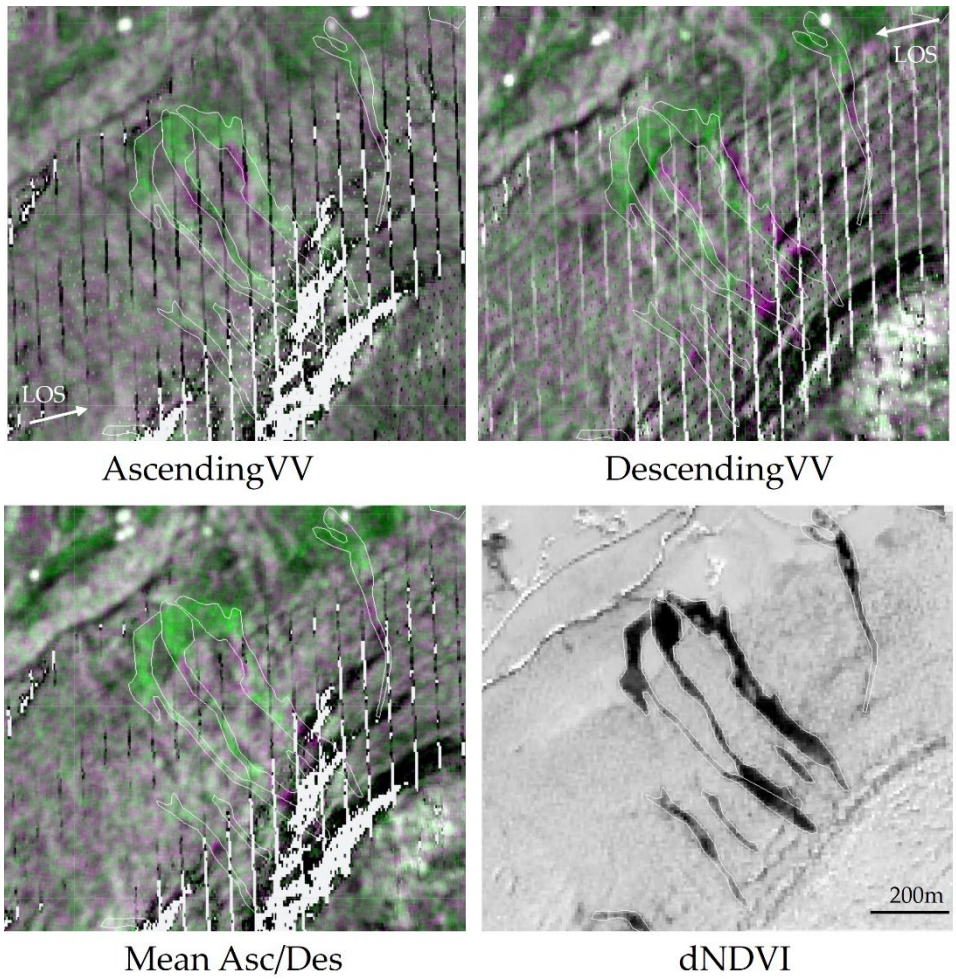

Figure 8. Landslides at Slåtten (subset A) in multi-temporal VV-polarised SAR backscatter intensity change images, (ascending, descending and mean) change in NDVI (bottom right). Green indicates backscatter intensity increase, purple indicates decrease. White outlines were mapped from the Sentinel-2 dNDVI image.

We believe in the case of S1-only, that the false negatives are due to the landslide expression in this location being different from other areas. Averaging the ascending and descending images tends to produce a final post-event image that shows mainly increased backscatter intensity in the area of the landslides. Yet here, the landslides are expressed in the input SAR images by decreased backscatter intensity, relative to the pre-event image. When viewed separately in ascending and descending images, landslides in forested areas show both decreased backscatter intensity on the side of the landslide nearest to the sensor, as well as a wide parallel band of increased backscatter intensity on the far side. It is possible that geometric distortions in the descending image and DEM distortions also affect the results. This can be seen in Figure 8.

We suspect that the performance of the classifier is strongly affected by the combination of ascending and descending images, due to the simplification of the landslide signature and averaging out of most areas with decreased backscatter intensity. This is important to note for others considering to follow this approach, as local vegetation conditions, landslide type and geometry, as well as slope orientation relative to the sensor can affect how landslides are expressed in SAR backscatter intensity data [50]. We did not test the U-net model using separate ascending and descending images as input; however this would be interesting to compare.

The DL model had a clear advantage over the ML model for the S1-only input data setting, with MCC scores of 73% and 20% respectively. The ML model could detect the changes due to landslides with only S1 data, however there were many false positives due to speckle noise. Whereas the DL model

Preprints (www.preprints.org) | NOT PEER-REVIEWED | Posted: 13 January 2023 doi:10.20944/preprints202301.0231.v1

uses a sliding window approach and is capable of differentiating speckle noise from landslide signatures.

Recommendations for an operational landslide detection system and future research.

Landslide detection and mapping is undertaken for different purposes, including (i) rapid emergency response; and (ii) inventory creation for use in spatial analyses (e.g., for hazard and susceptibility mapping, or deriving local thresholds for early warning), or verification and improvement of landslide early warnings. Each of these situations have different priorities for the timeliness and accuracy of landslide data needed. The recommendations based on the findings of this study and relevant literature are organised accordingly.

Rapid emergency response: the priority is to detect landslides as quickly as possible, while accurate delineation and mapping is of lower importance. In this situation, we recommend the use of SAR only models, as there is no need to wait for cloud-free conditions at the time of writing, no globally-trained SAR based landslide detection models are available. Therefore, a locally-trained model is needed. If a local landslide inventory of polygon data is available, then CNN models such as U-net give much higher performance than a conventional ML model due to their ability to differentiate speckle noise from landslide signatures. Using the methodology presented in this study, landslide predictions could be produced within three hours of the SAR image becoming available but requires computational power and a GPU. Where no local landslide inventory is available, the simple locally-trained ML approach using Google Earth Engine performed in this study, could be repeated for a new area in around 30 minutes after the image is available in GEE. This method requires only internet access and a free GEE account.

Inventory creation: the priority is for accurate and complete landslide data (including date, size information), while rapid detection is of lower importance. For automatically delineating landslides, optical or multispectral images, combined with terrain-corrected multi-temporal SAR data with best possible resolution are recommended. The locally-trained U-net DL approach gave the best performance in a glacial setting. The globally-trained models did not perform well in our study area due to shadows. Best performance would be achieved using images from a similar season and could be performed over large areas as an annual systematic survey. For obtaining date information, a time-series approach based on SAR data would be useful, as it is possible to back-date landslide occurrence when the location is known.

A continuous monitoring system for landslide detection requires further research. Particularly in terms of the spatial and temporal signatures of landslides in SAR data, and how these vary in different environmental settings. Compared to deforestation, the problem of landslide detection is more complex, because landslides can occur in a range of different land cover types. Ongoing developments in data availability and pre-processing of images will provide many more options to explore. These include the NISAR satellites due to be launched in 2023 with L and X band SAR capabilities [51]. Additionally, improvements to the pre-processing of the Sentinel-2 images may result in better predictions in the generalized ML models we tested.

In working towards developing a system for continuous detection of landslides over large areas, the GEE platform is very suitable, as multiple datasets (e.g., optical, SAR, soil moisture, precipitation, slope, land cover type) can be combined and analyses performed quickly over large areas. Furthermore, there is possibility to incorporate an external cloud based TensorFlow model, as used by Prakash et al, within the workflow. The CCDC model is designed for continuous monitoring. Modifying the CCDC model (e.g., using Sentinel data, and masking to show only vegetation loss) would be a good start. Training data should also include examples with areas likely to cause false negatives, e.g., with forestry or agricultural activity resulting in vegetation loss.

6. Conclusions

The locally-trained models outperformed the globally-trained models at detecting landslides in a glacial setting. The best result was achieved using the deep-learning approach with a U-net architecture, and input data including difference in NDVI (normalised difference vegetation index)

from Sentinel-2 and pre- and post-event SAR data (terrain-corrected, mean of multi-temporal ascending descending images, in VV polarisation) from Sentinel-1.

The generalized globally trained ML-based models did not perform very well for landslide detection in a glacial landscape. The model from Prakash, showed good potential to be applied in Norway, however it would require retraining and further development to perform well in the local conditions. The model performance could be improved by retaining including the NIR band which is more robust in shadow areas.

High rates of false negatives (missed landslides) were the main source of error for the CCDC, Tehrani and the Prakash-model run using Sentinel-2 Level-1C images. While the Prakash model runs using Sentinel-2 Level 2A images resulted in high rates of false positives, mainly due to over brightened artefacts on north facing slopes introduced by a terrain over correction. The results likely could be improved by a) rerunning the tests when the reprocessed data is released by Copernicus, b) including Norwegian training data and c) further development of the methods.

For development of an operational landslide detection system, a SAR-only based approach using a deep-learning model, is recommended for rapid detection as part of an emergency response. While for detailed mapping, and back-dating of landslides, a combination of SAR and optical data can give improved performance over optical data alone, and the time-series approaches can be used for continuous monitoring, or to back-date landslides.

Author Contributions: Conceptualization, Erin Lindsay (E.L.) Alexandra Jarna Ganerød (A.J.G.); methodology, E.L and A.J.G; software, E.L and A.J.G; validation, E.L. and A.J.G; formal analysis, E.L. and A.J.G.; investigation, E.L. and A.J.G; resources, E.L., data curation, E.L. and A.J.G.; writing—original draft preparation, E.L. and A.J.G; writing—review and editing, E.L., A.J.G and Ola Fredin (O.F.), Tor-Andre Myrvoll (O-A.M.), Steinar Nordal (S.N.), Jan Ketil Rød (J.K.R.); visualization, E.L A.J.G; supervision, O.F, T.-A.M., S.N. and J.K.R. All authors have read and agreed to the published version of the manuscript.

Funding: This research was funded by the Research Council of Norway and several partners through the Centre for Research-based Innovation 'Klima 2050' (Grant No 237859) (see www.klima2050.no), as well as through the Norwegian Geotechnical Institute through its basic funding from the Norwegian Government (GBV 2020 & 2021).

Data Availability Statement: Scripts used for the locally-trained models will be uploaded to GitHub.

Acknowledgments: Paulo Arevalo for providing the CCDC results for our study area. This paper contains modified Copernicus Sentinel data [2020] processed by Sentinel Hub, and Planet Scope Data provided by the European Space Agency and Planet under project: 61234 - Landslide detection using satellite data. Gabriela Spakman-Tanasescu for introducing the possibilities of ArcGIS Pro and deep learning.

Conflicts of Interest: "The authors declare no conflict of interest".

References

1. Wallemacq, P.; Below, R.; McClean, D. *Economic Losses, Poverty & Disasters: 1998-2017*; House, R., Ed.; United Nations Office for Disaster Risk Reduction: Geneva, Switzerland, 2018;
2. Piciullo, L.; Calvello, M.; Cepeda, J.M. Territorial Early Warning Systems for Rainfall-Induced Landslides. *Earth-Science Reviews* 2018.
3. Shano, L.; Raghuvanshi, T.K.; Meten, M. Landslide Susceptibility Evaluation and Hazard Zonation Techniques – a Review. *Geoenvironmental Disasters* **2020**, *7*, 18, doi:10.1186/s40677-020-00152-0.
4. Guzzetti, F.; Mondini, A.C.; Cardinali, M.; Fiorucci, F.; Santangelo, M.; Chang, K.-T. Landslide Inventory Maps: New Tools for an Old Problem. *Earth-Science Reviews* **2012**, *112*, 42–66, doi:10.1016/J.EARSCIREV.2012.02.001.
5. Tehrani, F.S.; Calvello, M.; Liu, Z.; Zhang, L.; Lacasse, S. Machine Learning and Landslide Studies: Recent Advances and Applications. *Natural Hazards* **2022**, *114*, 1197–1245, doi:10.1007/s11069-022-05423-7.
6. Reiche, J.; Mullissa, A.; Slagter, B.; Gou, Y.; Tsendbazar, N.-E.; Odongo-Braun, C.; Vollrath, A.; Weisse, M.J.; Stolle, F.; Pickens, A.; et al. Forest Disturbance Alerts for the Congo Basin Using Sentinel-1. *Environmental Research Letters* **2021**, *16*, 24005.
7. Hansen, M.C.; Krylov, A.; Tyukavina, A.; Potapov, P. V; Turubanova, S.; Zutta, B.; Ifo, S.; Margono, B.; Stolle, F.; Moore, R. Humid Tropical Forest Disturbance Alerts Using Landsat Data. *Environmental Research Letters* **2016**, *11*, 34008.

8. Vargas, C.; Montalban, J.; Leon, A.A. Early Warning Tropical Forest Loss Alerts in Peru Using Landsat. *Environmental Research Communications* **2019**, *1*, 121002.
9. Katiyar, V.; Tamkuan, N.; Nagai, M. Near-Real-Time Flood Mapping Using off-the-Shelf Models with SAR Imagery and Deep Learning. *Remote Sensing* **2021**, *13*, 2334.
10. Ban, Y.; Zhang, P.; Nascetti, A.; Bevington, A.R.; Wulder, M.A. Near Real-Time Wildfire Progression Monitoring with Sentinel-1 SAR Time Series and Deep Learning. *Scientific reports* **2020**, *10*, 1–15.
11. Zhang, P.; Ban, Y.; Nascetti, A. Learning U-Net without Forgetting for near Real-Time Wildfire Monitoring by the Fusion of SAR and Optical Time Series. *Remote Sensing of Environment* **2021**, *261*, 112467.
12. Devoli, G.; Bell, R.; Cepeda, J. *Susceptibility Map at Catchment Level, to Be Used in Landslide Forecasting, Norway*; Oslo, 2019;
13. Zhu, Z.; Woodcock, C.E. Continuous Change Detection and Classification of Land Cover Using All Available Landsat Data. *Remote Sensing of Environment* **2014**, *144*, 152–171, doi:https://doi.org/10.1016/j.rse.2014.01.011.
14. Arévalo, P.; Bullock, E.L.; Woodcock, C.E.; Olofsson, P. A Suite of Tools for Continuous Land Change Monitoring in Google Earth Engine. *Frontiers in Climate* **2020**, *2*, doi:10.3389/fclim.2020.576740.
15. Prakash, N.; Manconi, A.; Loew, S. A New Strategy to Map Landslides with a Generalized Convolutional Neural Network. *Scientific Reports* **2021**, *11*, 9722, doi:10.1038/s41598-021-89015-8.
16. Ghorbanzadeh, O.; Gholamnia, K.; Ghamisi, P. The Application of ResU-Net and OBIA for Landslide Detection from Multi-Temporal Sentinel-2 Images. *Big Earth Data* **2022**, 1–26, doi:10.1080/20964471.2022.2031544.
17. Nava, L.; Bhuyan, K.; Meena, S.R.; Monserrat, O.; Catani, F. *Assessment of Deep Learning Based Landslide Detection and Mapping Performances with Backscatter SAR Data*; 2022;
18. Bai, L.; Li, W.; Xu, Q.; Peng, W.; Chen, K.; Duan, Z.; Lu, H. Multispectral U-Net: A Semantic Segmentation Model Using Multispectral Bands Fusion Mechanism for Landslide Detection. **2022**.
19. Dong, Z.; An, S.; Zhang, J.; Yu, J.; Li, J.; Xu, D. L-Unet: A Landslide Extraction Model Using Multi-Scale Feature Fusion and Attention Mechanism. *Remote Sensing* **2022**, *14*, 2552.
20. Fang, C.; Fan, X.; Zhong, H.; Lombardo, L.; Tanyas, H.; Wang, X. A Novel Historical Landslide Detection Approach Based on LiDAR and Lightweight Attention U-Net. *Remote Sensing* **2022**, *14*, 4357.
21. Nava, L.; Monserrat, O.; Catani, F. Improving Landslide Detection on SAR Data Through Deep Learning. *IEEE Geoscience and Remote Sensing Letters* **2022**, *19*, 1–5, doi:10.1109/LGRS.2021.3127073.
22. Kamiyama, J.; Noro, T.; Sakagami, M.; Suzuki, Y.; Yoshikawa, K.; Hikosaka, S.; Hirata, I. Detection of Landslide Candidate Interference Fringes in DInSAR Imagery Using Deep Learning. *Recall* **2018**, *90*, 94–95.
23. Mondini, A.C.; Guzzetti, F.; Chang, K.-T.; Monserrat, O.; Martha, T.R.; Manconi, A. Landslide Failures Detection and Mapping Using Synthetic Aperture Radar: Past, Present and Future. *Earth-Science Reviews* **2021**, *216*, 103574, doi:https://doi.org/10.1016/j.earscirev.2021.103574.
24. Bullock, E.L.; Healey, S.P.; Yang, Z.; Houborg, R.; Gorelick, N.; Tang, X.; Andrianirina, C. Timeliness in Forest Change Monitoring: A New Assessment Framework Demonstrated Using Sentinel-1 and a Continuous Change Detection Algorithm. *Remote Sensing of Environment* **2022**, *276*, 113043.
25. Doblas, J.; Reis, M.S.; Belluzzo, A.P.; Quadros, C.B.; Moraes, D.R. V; Almeida, C.A.; Maurano, L.E.P.; Carvalho, A.F.A.; Sant'Anna, S.J.S.; Shimabukuro, Y.E. DETER-R: An Operational near-Real Time Tropical Forest Disturbance Warning System Based on Sentinel-1 Time Series Analysis. *Remote Sensing* **2022**, *14*, 3658.
26. Shumilo, L.; Kussul, N.; Lavreniuk, M. U-Net Model for Logging Detection Based on the Sentinel-1 and Sentinel-2 Data. In Proceedings of the 2021 IEEE International Geoscience and Remote Sensing Symposium IGARSS; 2021; pp. 4680–4683.
27. Kirschbaum, D.B.; Adler, R.; Hong, Y.; Hill, S.; Lerner-Lam, A. A Global Landslide Catalog for Hazard Applications: Method, Results, and Limitations. *Natural Hazards* **2010**, *52*, 561–575, doi:10.1007/s11069-009-9401-4.
28. Breiman, L.; Friedman, J.H.; Olshen, R.A.; Stone, C.J. *Classification and Regression Trees*; Routledge, 2017;
29. NGU Landslides.
30. Luigi, S.; Guzzetti, F. Earth-Science Reviews Landslides in a Changing Climate. *Earth Science Reviews* **2016**, *162*, 227–252, doi:10.1016/j.earscirev.2016.08.011.
31. Herrera, G.; Mateos, R.M.; Garcia-Davalillo, J.C.; Grandjean, G.; Poyiadji, E.; Maftei, R.; Filipciuc, T.-C.; Auflič, M.J.; Jež, J.; Podolszki, L.; et al. Landslide Databases in the Geological Surveys of Europe. *Landslides* **2018**, *15*, 359–379.
32. Jaedicke, C.; Lied, K.; Kronholm, K. Integrated Database for Rapid Mass Movements in Norway. **2009**.
33. Malamud, B.D.; Heijenk, R.A.; Taylor, F.E.; Wood, J.L. *Road Influences on Landslide Inventories*; 2022;
34. Ruther, D.C.; Hefre, H.; Rubensdotter, L. Extreme Precipitation-Induced Landslide Event on 30th 3 July 2019 in Jølster, Western Norway. *NORWEGIAN JOURNAL OF GEOLOGY* **2022**.

35. Lindsay, E.; Frauenfelder, R.; Rüther, D.; Nava, L.; Rubensdotter, L.; Strout, J.; Nordal, S. Multi-Temporal Satellite Image Composites in Google Earth Engine for Improved Landslide Visibility: A Case Study of a Glacial Landscape. *Remote Sensing* **2022**, *14*, doi:10.3390/rs14102301.
36. Devoli, G.; Colleuille, H.; Sund, M.; Wasrud, J. Seven Years of Landslide Forecasting in Norway---Strengths and Limitations. In *Understanding and Reducing Landslide Disaster Risk: Volume 3 Monitoring and Early Warning*; Casagli, N., Tofani, V., Sassa, K., Bobrowsky, P.T., Takara, K., Eds.; Springer International Publishing: Cham, 2021; pp. 257–264 ISBN 978-3-030-60311-3.
37. Hanssen-Bauer, I.; Drange, H.; Førland, E.J.; Roald, L.A.; Børsheim, K.Y.; Hisdal, H.; Lawrence, D.; Nesje, A.; Sandven, S.; Sorteberg, A.; et al. Climate in Norway 2100. *Background information to NOU Climate adaptation (In Norwegian: Klima i Norge 2100. Bakgrunnsmateriale til NOU Klimatilplassing), Oslo: Norsk klimasenter* **2009**.
38. Herrera Herrera, M. Landslide Detection Using Random Forest Classifier, Delft University of Technology, 2019.
39. Vollrath, A.; Mullissa, A.; Reiche, J. Angular-Based Radiometric Slope Correction for Sentinel-1 on Google Earth Engine. *Remote Sensing* **2020**, *12*, doi:10.3390/rs12111867.
40. Ronneberger, O.; Fischer, P.; Brox, T. U-Net: Convolutional Networks for Biomedical Image Segmentation. In Proceedings of the Medical Image Computing and Computer-Assisted Intervention -- MICCAI 2015; Navab, N., Hornegger, J., Wells, W.M., Frangi, A.F., Eds.; Springer International Publishing: Cham, 2015; pp. 234–241.
41. Huang, S.-C.; Le, T.-H. Introduction to TensorFlow 2. In *Principles and Labs for Deep Learning*; Elsevier, 2021; pp. 1–26.
42. Shelhamer, E.; Long, J.; Darrell, T. Fully Convolutional Networks for Semantic Segmentation. *IEEE Transactions on Pattern Analysis and Machine Intelligence* **2017**, *39*, 640–651, doi:10.1109/TPAMI.2016.2572683.
43. Ye, J.; Ni, J.; Yi, Y. Deep Learning Hierarchical Representations for Image Steganalysis. **2017**, *12*, 2545–2557.
44. Liu, Y.H. Feature Extraction and Image Recognition with Convolutional Neural Networks. *Journal of Physics: Conference Series* **2018**, *1087*, doi:10.1088/1742-6596/1087/6/062032.
45. Chicco, D.; Jurman, G. The Advantages of the Matthews Correlation Coefficient (MCC) over F1 Score and Accuracy in Binary Classification Evaluation. **2020**, 1–13.
46. Clerc, S.; MPC-Team Terrain Over-Correction on Shaded Areas. In *S2 MPC Level 2A Data Quality Report*; ESA, 2022; Vol. 45, p. 28.
47. Jackson, J. Clarification on Difference between L1C and L2A Data.
48. Ghorbanzadeh, O.; Blaschke, T.; Gholamnia, K.; Meena, S.R.; Tiede, D.; Aryal, J. Evaluation of Different Machine Learning Methods and Deep-Learning Convolutional Neural Networks for Landslide Detection. *Remote Sensing* **2019**, *11*, doi:10.3390/rs11020196.
49. Prakash, N.; Manconi, A.; Loew, S. Mapping Landslides on EO Data: Performance of Deep Learning Models vs. Traditional Machine Learning Models. *Remote Sensing* **2020**, *12*, doi:10.3390/rs12030346.
50. Lindsay, E.; Devoli, G.; Reiches, J.; Nordal, S. In Progress: Spatial and Temporal Signatures of Landslides in C-Band SAR Data. **2023**.
51. NASA Quick Facts.